Research Article

Ali Mohammadpour-Haratbar, Behrooz Mosallanejad, Yasser Zare*, Kyong Yop Rhee*, and Soo-Jin Park*

Co_3O_4 nanoparticles embedded in electrospun carbon nanofibers as free-standing nanocomposite electrodes as highly sensitive enzyme-free glucose biosensors

https://doi.org/10.1515/rams-2022-0251
received June 06, 2022; accepted June 27, 2022

Abstract: Numerous researches have been directed toward enzyme-free biosensors to alleviate the shortcomings encountered with enzymatic biosensors, in particular the intricate enzyme immobilization procedure. Herein, Co_3O_4/electrospun carbon nanofiber (ECNF) nanocomposites are successfully prepared to be employed as enzyme-free biosensors for diagnosis of glucose. Two parameters including the carbonization time and the amount of Cobalt(II) acetate tetrahydrate precursor are optimized, which are 5 h and 0.5 g, respectively. The 0.5 Co_3O_4/ECNF-5 h nanocomposite delivers superior sensitivity (475.72 $\mu A \cdot mM^{-1} \cdot cm^{-2}$), broad linear range (2–10 mM), and detection limit (LOD) less than 1 mM (0.82 Mm). In addition, the electrode shows excellent selectivity. The chronoamperometric analysis of 0.5 Co_3O_4/ECNF-5 h nanocomposite is performed by adding successively glucose analyte and interfering agents to the 0.1 M sodium hydroxide solution. No significant amperometric signal to the interfering agents including uric acid, ascorbic acid, and dopamine is delivered by this electrode, testifying the great selectivity of the electrode toward the diagnosis of target analyte (glucose) in spite of the existence of interfering species. Taking the aforementioned explanations into account, it can be concluded that the Co_3O_4/ECNF nanocomposite can be an appropriate free-stand electrode for high-performance enzyme-free glucose biosensor.

Keywords: electrospun carbon nanofibers, enzyme-free glucose biosensor, Co_3O_4 nanoparticles, electrochemical biosensor

1 Introduction

Diabetes as a metabolic disease is one of the main world health problems that can result in many health complications, including heart disease, amputation, renal failure, blindness, disability, and mortality [1–3]. Owing to their high sensitivity, simplicity in their construction and being cost-effective, electrochemical biosensors have been considered the reliable means to detect the dose of glucose in human blood [4–6]. Electrochemical biosensors are classified into two prime groups: enzymatic and nonenzymatic biosensors [7]. The former benefits from superior selectivity, rapid performance, and good catalytic activity. But, some handicaps, consisting of the complex immobilization procedure of the glucose oxidase (GOx) enzyme, the effect of temperature, pH, and humidity on the electrocatalytic performance of GOx and the high cost of this enzyme have hindered the further development of enzymatic biosensors [8,9]. Hence, the recent research has hugely been concentrated on enzyme-free biosensors to mitigate the shortcomings encountered with the enzymatic biosensors [10–12].

The studies on enzyme-free glucose sensors largely revolved around the direct response of glucose oxidation on the electrode [13]. Thus, the electrocatalytic activity of

* **Corresponding author: Yasser Zare,** Biomaterials and Tissue Engineering Research Group, Department of Interdisciplinary Technologies, Breast Cancer Research Center, Motamed Cancer Institute, ACECR, Tehran, Iran, e-mail: y.zare@aut.ac.ir
* **Corresponding author: Kyong Yop Rhee,** Department of Mechanical Engineering (BK21 four), College of Engineering, Kyung Hee University, Yongin, Republic of Korea, e-mail: rheeky@khu.ac.kr
* **Corresponding author: Soo-Jin Park,** Department of Chemistry, Inha University, Incheon 22212, Republic of Korea, e-mail: sjpark@inha.ac.kr
Ali Mohammadpour-Haratbar: Department of Polymer Engineering & Color Technology, Amirkabir University of Technology, Tehran, Iran
Behrooz Mosallanejad: Department of Chemistry, Amirkabir University of Technology, Tehran, Iran

the electrode material is one of the major parameters regarding the enzyme-free glucose sensors' performance, which impacts their selectivity and sensitivity [3]. With the significant progress made in nanoscience and nanotechnology, new approaches have been introduced for the progression of enzyme-free biosensors for the diagnosis of glucose. In this regard, various nanostructured electrocatalysts have been developed to be adopted as enzyme-free glucose sensors, one of which is hybrid system made up of carbon-based nanomaterials and metal nanoparticles [1,8]. The latter not only are used as substrates for electrocatalysts but also provide them with large surface area, which simplify the charge transfer and fast electron transfer, giving rise to an increment in the biosensors's sensitivity [14,15].

One of the most effective approaches to fabricate nanofibers holding diameters ranging from nanometers to microns is electrospinning [16,17]. In addition, this technique is facile, straightforward, and fast for the production of nanofibers [18,19]. Some features, including high specific surface area and high conductivity, have made electrospun nanofibers an appropriate candidate for an extensive range of applications [20,21].

The development of nanotechnology has resulted in the development of a number of nanomaterials with unique properties, such as optical, electrical, and mechanical [22]. In recent years, carbon nanomaterials such as graphene and its derivatives, carbon nanotubes, and carbon nanofibers have been used in a variety of applications due to their high electrical conductivity and high specific surface area [23–26]. Among the conductive carbon-based nanomaterials, electrospun carbon nanofibers (ECNFs) can be employed as a substrate to anchor electrocatalysts to be used as electrochemical biosensors [27]. One of the features distinguishing ECNFs from other types of carbon-based nanomaterials is that they can be utilized directly as free-stand electrodes without the need for any binder, which leads to the increasing of the conductivity of the electrodes [15,28]. Metal nanoparticles are considered electronic wires and electrocatalysts due to their nanosized structure and their role in providing fast electron transfer between the transducer and analyte molecules [29,30]. The electrocatalysts based on noble metals like Pt and Au show high performance toward glucose oxidation [31]. But these materials are expensive, and their electrocatalytic activity is adversely influenced by adsorption and accumulation of intermediates or chloride ions [32,33]. Hence, considerable efforts have been made to develop highly selective, sensitive, cost-effective, trustworthy, and fast electrocatalysts, which can be pointed out nanoscale metal oxides [34]. Some merits, including low cost, benignity to environment, relatively good conductivity, and electrocatalytic properties, have made Co_3O_4 nanoparticles as a suited material for enzyme-free glucose sensing [12,14,35].

In this research, an electrospinning technique combined with a heat treatment process was hired to synthesize Co_3O_4/ECNF nanocomposites to use as high-performance electrodes for biosensors. The nanocomposites were structurally studied using field emission scanning electron microscopy, X-ray diffraction (XRD), X-ray photoelectron spectroscopy (XPS), Raman spectroscopy, and thermogravimetric analysis (TGA). The electrochemical properties of the composite electrodes for glucose detection were also analyzed using cyclic voltammetry (CV), chronoamperometric (CA), and electrochemical impedance spectroscopy (EIS) tests.

2 Experiment

2.1 Chemicals and reagents

Polyacrylonitrile (PAN) with an average molecular weight of 80,000 $g \cdot mol^{-1}$ as ECNF matrix source was purchased from Polyacryle Company (Iran). Cobalt(II) acetate tetrahydrate (CoAc) as a Co source was provided from Sigma Aldrich Company. *N,N*-Dimethylformamide (DMF) as a solvent of electrospinning solution was purchased from Fluka Company. Glucose and sodium hydroxide (NaOH) used as the analyte and the electrolyte in electrochemical reactions were purchased from Mojalaly Company (Iran).

2.2 Synthesis procedure of Co_3O_4/ECNF

The Co_3O_4/ECNF nanocomposites were synthesized based on the carbonization process of CoAc/PAN nanofibers as in our previous work [36]. In this regard, the dissolvation of 12 wt% of PAN was first done in DMF at environment temperature under vigorous stirring for 2 h. Then, 5 wt% CoAc was included in the prepared solution and stirred overnight. A plastic syringe was filled with the solution, and it was then electrospun using an electrospinning device. 12 kV was applied during the electrospinning process. In addition, the distance between the collector and the spinneret was 10 cm, and the feeding rate was 0.5 $mL \cdot h^{-1}$. The resulting product was CoAc/PAN nanofiber. Afterward, CoAc/PAN nanofibers were stabilized at 250°C for 2 h in

a box furnace. In the carbonization step, stabilized electrospun fibers were carbonized in a tubular furnace under nitrogen gas at 800°C for 5 h, which were transformed into the Co/ECNF nanocomposite. Finally, a postheating treatment was done on the Co/ECNF at 320°C for 0.5 h in a box furnace under air and Co_3O_4/ECNF nanocomposites were obtained. Different carbonization times were selected to investigate the effect of carbonization time on the morphological structure of nanofibers, including 1, 3, and 5 h, and the resulting products were, respectively, named as 0.5 Co_3O_4/ECNF-1 h, 0.5 Co_3O_4/ECNF-3 h, and 0.5 Co_3O_4/ECNF-5. In addition, to optimize the compositions, various amounts of CoAc precursor were added to the PAN/DMF solution, namely, 2, 3.5, 5, and 6.5 wt%. The viscosity of the electrospinning solution containing 6.5 wt% CoAc was very low, and no fiber was formed on the collector. Therefore, for other amounts of CoAc, consisting of 0.2, 0.35, and 0.5 g, the final nanofibers were labeled as 0.2 Co_3O_4/ECNF-5 h, 0.35 Co_3O_4/ECNF-5 h, and 0.5 Co_3O_4/ECNF-5 h, respectively. As well, pure ECNF was synthesized using the same procedure from 12 wt% PAN without the inclusion of CoAc.

2.3 Morphological and Structural Characterization

Field emission-scanning electron microscopy (FESEM) (Mira 3-XMU, TESCAN Co.) test was used to examine the morphology of the nanocomposites. The determination of atomic percentage and identification of elements were carried out by the EDS analysis. The crystal structure of the nanocomposites was assessed by the XRD test using Cu Kα radiation (microanalyzerxmf-104). To evaluate the surface chemistry of the samples, XPS (Surface analysis PHI5600, Physical Electronics) was employed with a monochromatic Al Kα X-ray at 14 kV. Raman spectroscopy (LabRam HRUV) was used to examine the defects and degree of graphitization of ECNF-based nanocomposites. TGA (STA 504) under air was used to determine the amount of cobalt nanoparticles loaded into the ECNF matrix under conditions of 25–1,000°C at a heating rate of 10°C·min^{-1}. Electrical conductivity of the nanocomposites was calculated by a two-point probe (Source Meter Instrument Keithley) at room temperature.

2.4 Electrochemical properties

The electrochemical analyses were conducted using a three-electrode setup and 0.1 M NaOH as the electrolyte at environment temperature. Platinum and Ag/AgCl electrodes were adopted as auxiliary and reference electrodes, respectively. A free-standing electrode was fabricated without the use of a binder in specific dimensions using Co_3O_4/ECNF nanocomposites. Electrochemical evaluation of the prepared electrodes was carried out with CV and CA methods on an electrochemical workstation (Autolab PG STAT302 N). The measurements were done using various scan rates in a potential range of 0.2–0.8 V. EIS was also used to examine the electrode's resistance, which was performed in a frequency ranging from 10^{-2} to 10^5 Hz. Moreover, 5 mV was set as the alternating current (AC) voltage amplitude, and the measurement was performed in 0.1 M KCl electrolyte, including 6 mM $[Fe(CN)_6]^{3-/4-}$. Electrodes' sensitivity, linear range (LR), and LOD were determined using linear regression. The LR was calculated in the range of glucose concentrations where the current response is linear. All obtained electrodes had a cross-section of 0.6 cm^2. In addition, the LOD of the electrodes was calculated by equation (1) [37].

$$\mathrm{LOD} = 3.3S_a/S, \tag{1}$$

where S_a is the standard deviation of the blank signal and S is the slope of the calibration curve.

3 Results and discussion

3.1 Morphological and structural characteristics of Co_3O_4/ECNF nanocomposites

The FESEM images of the samples are depicted in Figure 1. The synthesized nanofibers show nanometer diameters and micron lengths (see Figure 1a). In addition, according to Figure 1b–f, the Co_3O_4/ECNF nanofibers have been uniformly synthesized with different amounts of CoAc salt and different carbonization times without any beads. The analysis of image processing performed by Image J Software revealed that fiber diameters vary from 250 to 450 nm. Moreover, a number of small nanoparticles are found on the ECNF surface, which are cobalt oxide nanoparticles (Figure 1c). Electrospinning produced PAN nanofibers infused with the cobalt acetate salt. The main mechanism involved in the formation of cobalt oxide nanoparticles from primary cobalt acetate salt is that during the carbonation process at temperatures between 250 and 500°C, cobalt acetate decomposes, allowing the acetate ligand to be separated under heat stress [38].

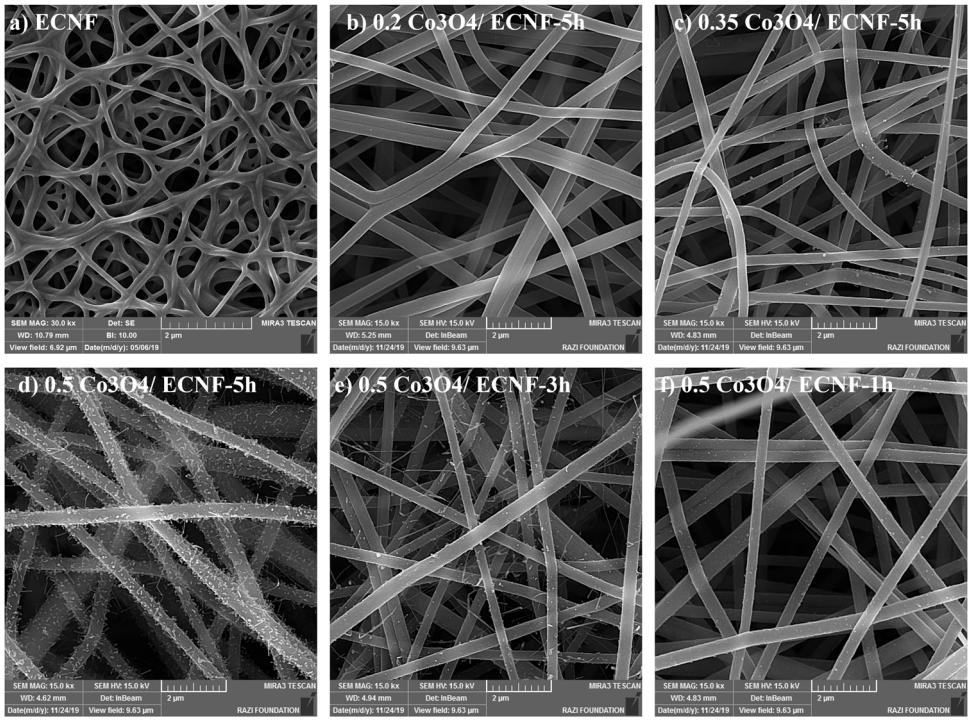

Figure 1: FESEM images of (a) ECNF, (b–d) Co_3O_4/ECNF nanocomposites with different amounts of CoAC salt, and (e and f) Co_3O_4/ECNF nanocomposites with different carbonization times.

Due to the concentration gradient of cobalt between the bulk and the ECNF surface, cobalt atoms migrated from the bulk to the ECNF surface [39]. After the carbonization step, the fibers underwent a postheating step, which converted the cobalt atoms on the ECNF surface to cobalt oxide. The number of cobalt oxide nanoparticles and their dispersion state depend on the amount of cobalt acetate precursor added to the electrospinning solution, as well as the temperature and the time of the carbonization process.

Figure 1b–d illustrate that the number of particles on the carbon surface increases as the amount of cobalt acetate increases. Also, by selecting different carbonization times of 1, 3, and 5 h, it is observed that the number of particles on the ECNF surface increases as carbonization time increases. Thus, the sample with 0.5 Co_3O_4/ECNF shows the best dispersion state, making it the optimal sample (Figure 1d–f). By processing the image, the diameter of particles of cobalt oxide on the ECNF surface was calculated, which was in the range of 60–85 nm.

The EDS diagram of the Co_3O_4/ECNF composite is shown in Figure 2a, which proves the presence of the elements of O, N, C, and Co. To verify the existence of Co_3O_4 and also to confirm the distribution of the Co element, the element mapping was conducted. Accordingly, the Co element was distributed uniformly (Figure 2b–d). Figure 2e manifests the XRD pattern of 0.5 Co_3O_4/ECNF-5h nanocomposite. The major peaks are located at 31.2, 36.8, 44.8, 59.3, and 65.2° ascribing, respectively, to the (220), (311), (400), (511), and (440) planes of Co_3O_4. Also, the peak situated at 2θ = 26.0° is imputed to the carbon (002) plane, implying that a graphite structure formed in the CO_3O_4/ECNF composite.

The formation of the graphitic structure in ECNF resulted in an increment in the structural order, which not only improves the electrical conductivity but also encapsulates Co_3O_4 nanoparticles within the ECNFs, thereby the separation of Co_3O_4 from the ECNF substrate is prevented [40].

Figure 3a shows the Raman spectra of Co_3O_4/ECNF nanocomposites containing different amounts of CoAc. Two main peaks situated at 1,319 and 1,589 cm^{-1} commonly appear in carbon materials, which correspond to the D and G bands of carbon, respectively [41]. The I_D/I_G ratio is used to determine the degree of graphitization, so the lower the ratio, the higher the degree of graphitization [42]. According to Table 1, the I_D/I_G ratio changed from 1.02 for 0.2 Co_3O_4/ECNF to 0.94 and 0.81, respectively, for 0.35 Co_3O_4/ECNF and 0.5 Co_3O_4/ECNF, meaning that with increasing the content of cobalt in the nanocomposite, the carbon graphitic layer grew and a

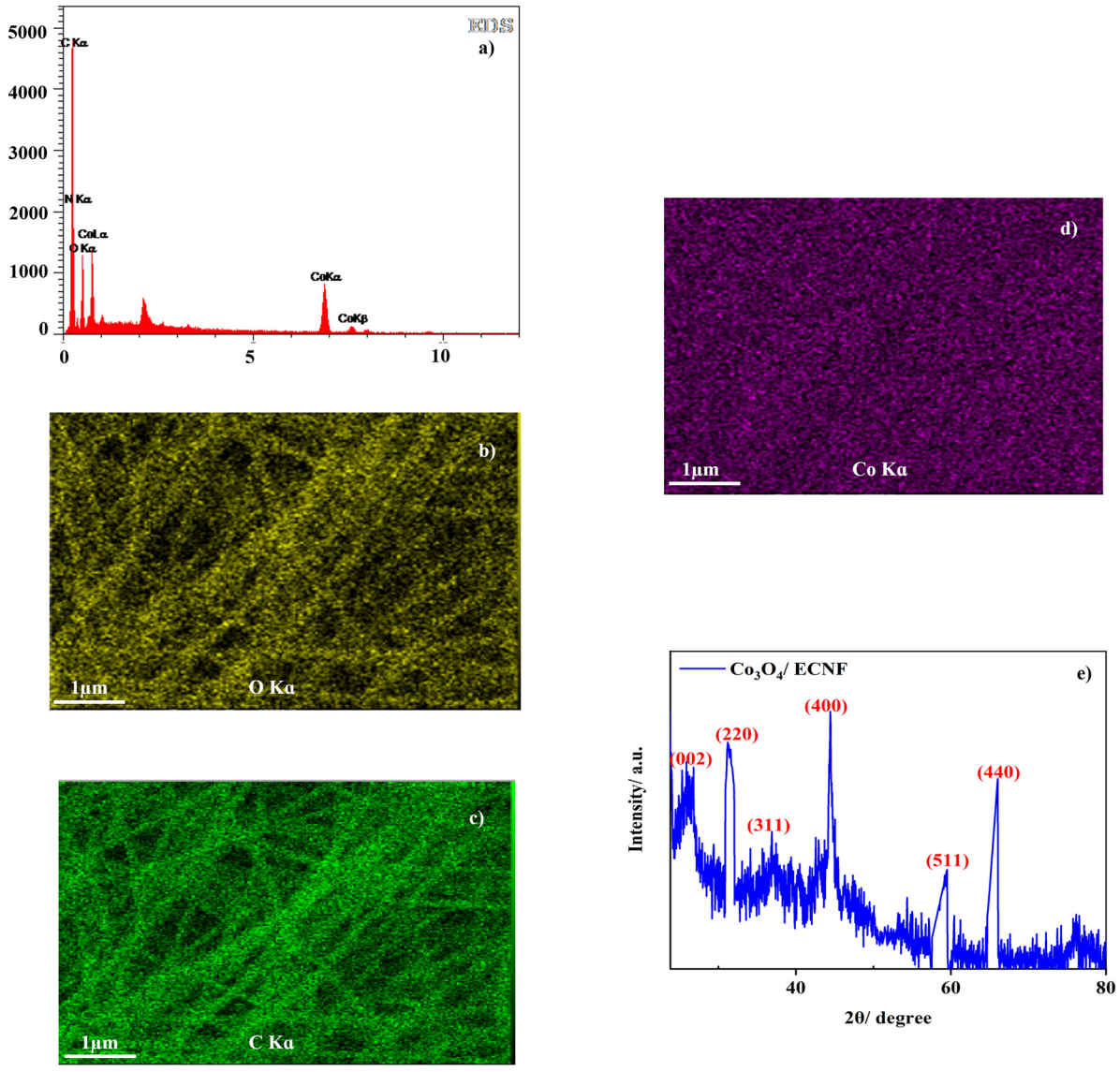

Figure 2: (a) EDS diagram; element mapping of (b) O, (c) C, and (d) Co; and (e) XRD of Co_3O_4/ECNF nanocomposite.

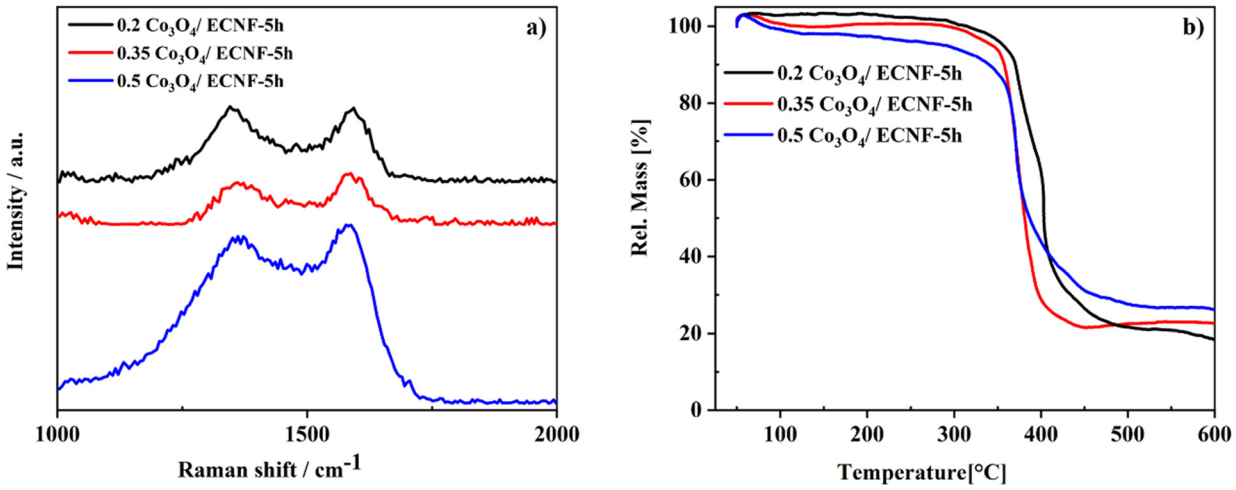

Figure 3: (a) Raman spectra and (b) TGA of Co_3O_4/ECNF nanocomposites with different amounts of CoAc.

decrease occurred in the spacing between two graphite layers. The reason behind it is that the presence of Co_3O_4 nanoparticles induced the localized heating during the pyrolysis process, which subsequently gives rise to the production of highly graphitized carbon fiber.

To further examine the effect of cobalt nanoparticles on the ECNF properties, the electrical conductivity of the composites was measured. Table 1 shows the conductivity of composites. Electrical conductivity is highest for sample 0.5 Co_3O_4/ECNF containing the largest amount of cobalt. In other words, when the amount of cobalt in the composite system increases, the graphite layer and degree of graphitization in ECNF increase, which facilitates electron transfer within the composite and increases electrical conductivity. Therefore, the electrical conductivity data are consistent with the Raman spectroscopy results.

Figure 3b shows the TGA curves obtained under air atmosphere for determining the composition of the composites. Accordingly, all the samples have a sharp weight loss at 300–400°C, which is related to the carbon oxidation reaction released as CO_2 gas [36]. Starting at 550°C, all nanocomposites achieved a continual weight accompanied with the remaining weight corresponding to the amount of Co_3O_4 present in each composite. As a result, the weight values of Co_3O_4 in 0.2 Co_3O_4/ECNF, 0.35 Co_3O_4/ECNF, and 0.5 Co_3O_4/ECNF are 19, 22.9, and 26.7 wt%, respectively.

XPS measurements were performed on Co_3O_4/ECNF-5h composite to assess the surface chemistry and chemical elements, and the results are shown in Figure 4. The general XPS spectrum in Figure 4a clearly shows that the Co_3O_4/ECNF is composed of C, O, N, and Co elements. Owing to the usage of PANs as the initial polymer material having N atom in their structure and also the carbonization process performed in nitrogen atmospheres, nitrogen is present. C-1s spectrum deconvoluted in Figure 4b shows three binding energies at 284.5, 285.4, and 288.1 eV, imputing to carbon sp^2 and sp^3, as well as the C–O functional group, respectively [40]. In Figure 4c, two well-defined peaks are observed at 779.8 and 781.4 eV, which are imputed to the Co $2p_{3/2}$ orbit of Co_3O_4. Furthermore, the presence of a satellite peak located around 787.6 eV further confirms the formation of the Co_3O_4 phase [43]. There are four peaks having the binding energies of 529.8, 531.3, 533.2, and 536.2 eV, which are ascribed to the O atoms in Co_3O_4, oxygen bands in C=O and C–O, and adsorbed surface water in the deconvoluted O 1s spectrum (Figure 4d) [40].

3.2 Electrocatalytic performance of glucose at the electrodes

The CV of the 0.5 Co_3O_4/ECNF-5h electrode with and without glucose is portrayed in Figure 5a. Two pairs of redox peaks can be detected in the CV curves arising from the redox reactions between Co_3O_4 and OH^- ions [44]. One of them is located at lower potential, which originates from the reversible transition between the Co_3O_4 and CoOOH (equation (2)). The other pair found at the higher potential stems from the redox reaction occurring between CoOOH and CoO_2 (equation (3)) [45–47].

$$Co_3O_4 + OH^- + H_2O \leftrightarrow 3CoOOH + e^-, \quad (2)$$

$$CoOOH + OH^- \leftrightarrow CoO_2 + H_2O + e^-, \quad (3)$$

$$2CoO_2 + C_6H_{12}O_6(\text{glucose}) \rightarrow 2CoOOH + C_6H_{10}O_6(\text{gluconolactone}). \quad (4)$$

It is worth mentioning that the addition of glucose resulted in an increment in the current density of the anodic peak, implying that the Co_3O_4 nanoparticles are capable of detecting of glucose. According to equation (4), oxidation of glucose leads to the production of gluconolactone as a result of a two-electron electrochemical reaction. During the oxidation reaction of glucose, the consumption and production of CoO_2 and CoOOH, respectively, take place, which is advantageous to the forward reaction of equation (2) and also the backward reaction of equation (3) because of the increment happening in the oxidation current at the higher potential and also in the reduction current at the lower potential, respectively [45,47]. The CV curves of the electrode in alkaline solutions containing various amounts of glucose varying from 2 to 10 mM are illustrated in Figure 5b.

Table 1: I_D/I_G ratio, degree of graphitization, and electrical conductivity of Co_3O_4/ECNF nanocomposites with different amounts of CoAc

Samples	I_D/I_G ratio	Degree of graphitization (%)	Electrical conductivity ($S \cdot cm^{-1}$)
0.2 Co_3O_4/ECNF	1.02	49.47	1.52
0.35 Co_3O_4/ECNF	0.94	51.63	5
0.5 Co_3O_4/ECNF	0.81	55.08	5.54

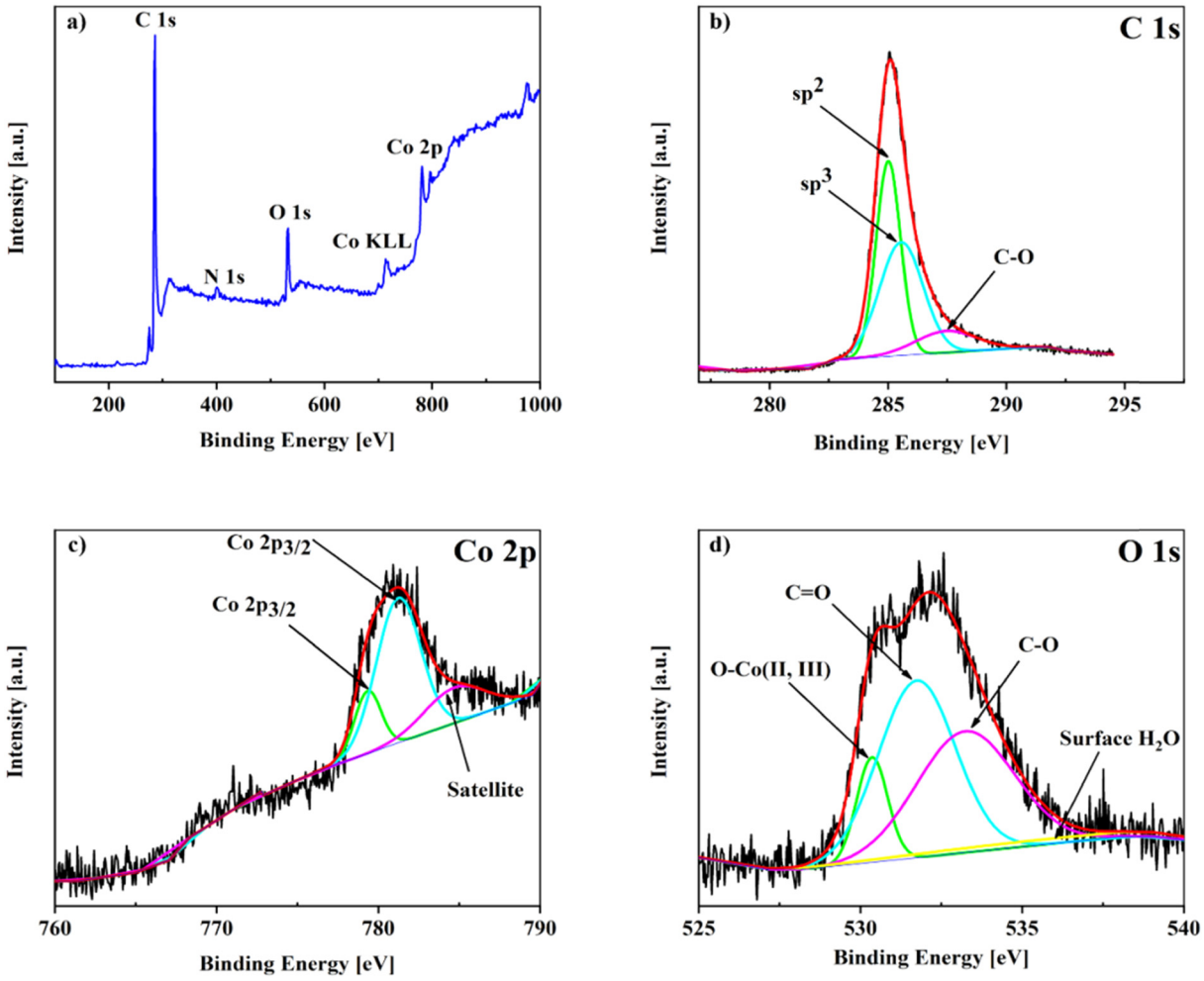

Figure 4: (a) General XPS spectrum and deconvoluted XPS spectra of (b) C 1 s, (c) Co 2p, and (d) O 1 s for 0.5 Co_3O_4/ECNF-5h nanocomposite.

Clearly, the increase in the glucose concentration led to the increase in the oxidation peak current, testifying the good sensitivity of the electrode toward the different concentrations of glucose. The CV curves of the electrode at various scan rates ranging from 20 to 200 $mV{\cdot}s^{-1}$ are depicted in Figure 5c. With increasing the scan rate, the redox peak currents increase. Figure 5d shows a linear relationship between the anodic and cathodic peak currents and the square root of the scan rate, indicating that a diffusion-controlled reaction is taking place during the redox reaction of glucose on the 0.5 Co_3O_4/ECNF-5 h electrode [25–27].

The Nyquist plots of the Co_3O_4/ECNF nanocomposites synthesized using various amounts of CoAc precursor, including 0.2, 0.35, and 0.5 g, are shown in Figure 6a. Each of the Nyquist plots comprises a small semicircle and also a straight line located, respectively, in the high-frequency and low-frequency zones. The semicircle is attributed to the electron transfer resistance (R_{ct}) determining the transfer kinetics of the electron at the electrode interface [47–49]. Among the samples, 0.5 Co_3O_4/ECNF-5 h electrode shows the lowest R_{ct}, implying the easiest electron transfer and the highest electron transfer rate in this electrode during the redox process. The straight line situated in the low-frequency zone denotes the Warburg impedance, attesting that the electrochemical reaction on the 0.5 Co_3O_4/ECNF-5h electrode is the diffusion-controlled process [48–50]. As a consequence, the EIS results are in cohesive with the CV analysis.

To opt an optimal potential applied during the amperometric experiments of glucose, the impacts of varied applied potentials in the range of 0.3–0.65 V were tested on the amperometric signal of the 0.5 Co_3O_4/ECNF-5 h electrode in an alkaline solution containing 4.0 mM glucose. As evidenced by Figure 6b, the maximum current was achieved at 0.55 V. To this end, this value was considered the optimal applied potential for amperometric measurements.

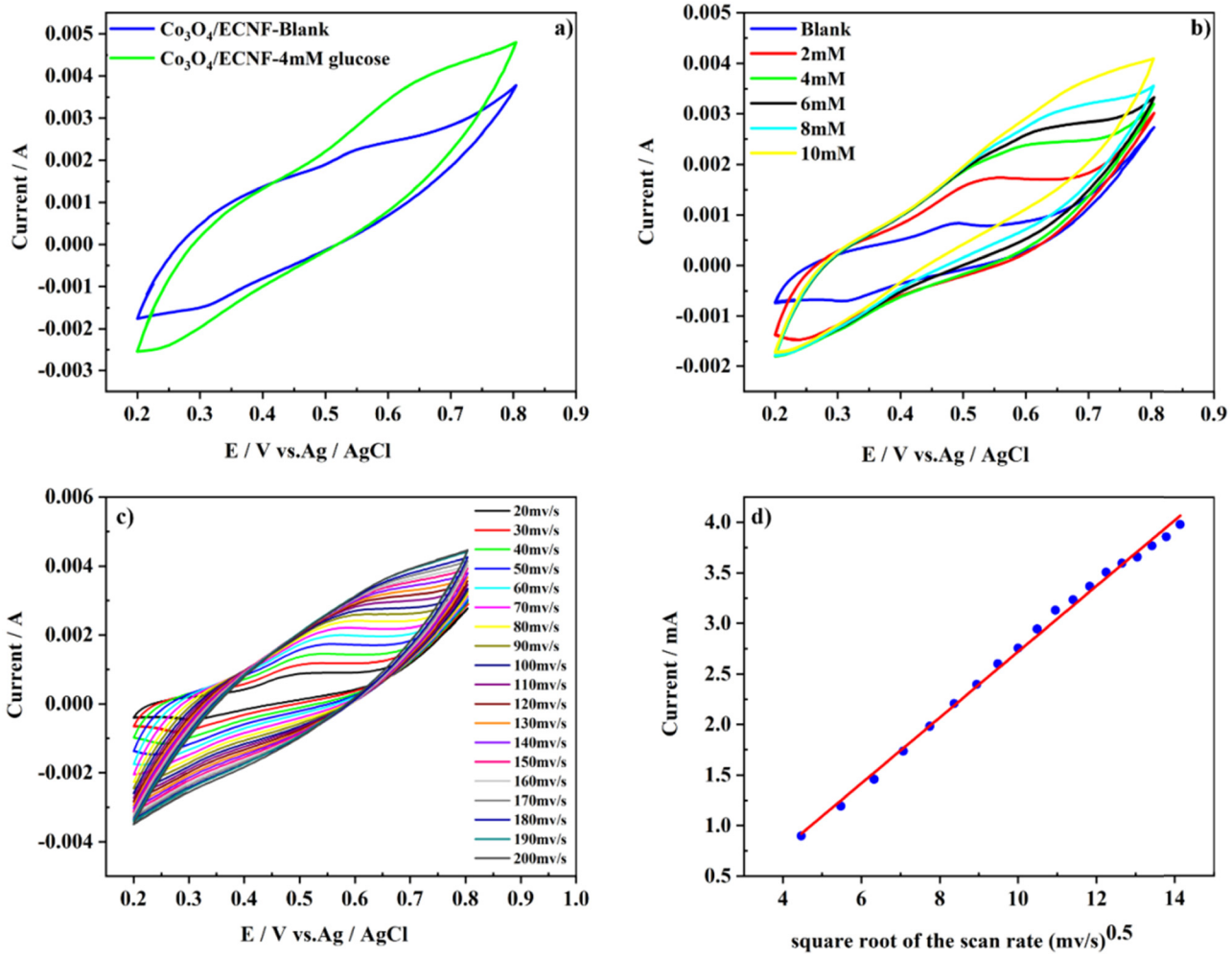

Figure 5: (a) and (b) Cyclic voltammogram of 0.5 Co_3O_4/ECNF-5h in the absence (Blank) and presence of analyte glucose with the scan rate as 50 mV·s^{-1} in a 0.1 M NaOH solution, (c) cyclic voltammogram of 4.0 mM glucose at 0.5 Co_3O_4/ECNF-5 h with different scan rates ranging from 20 to 200 mV·s^{-1} in a 0.1 M NaOH solution, and (d) the calibration curve of the current vs the square root of the scan rate.

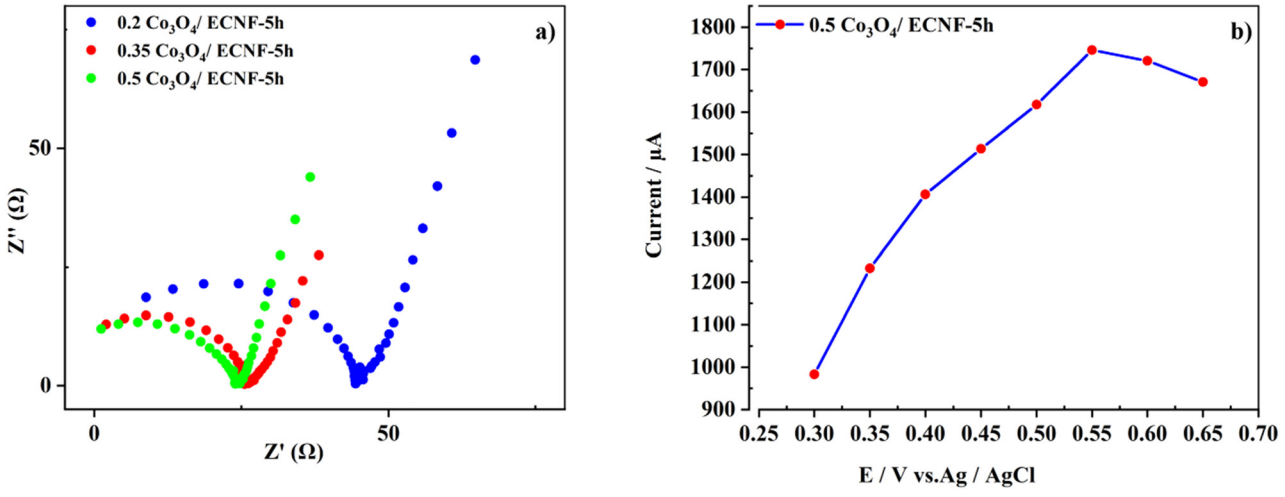

Figure 6: (a) EIS patterns of Co_3O_4/ECNF nanocomposites, and (b) effects of applied potential on the amperometric response of the 0.5 Co_3O_4/ECNF-5h electrode in 0.1 M NaOH solution containing 4.0 mM glucose.

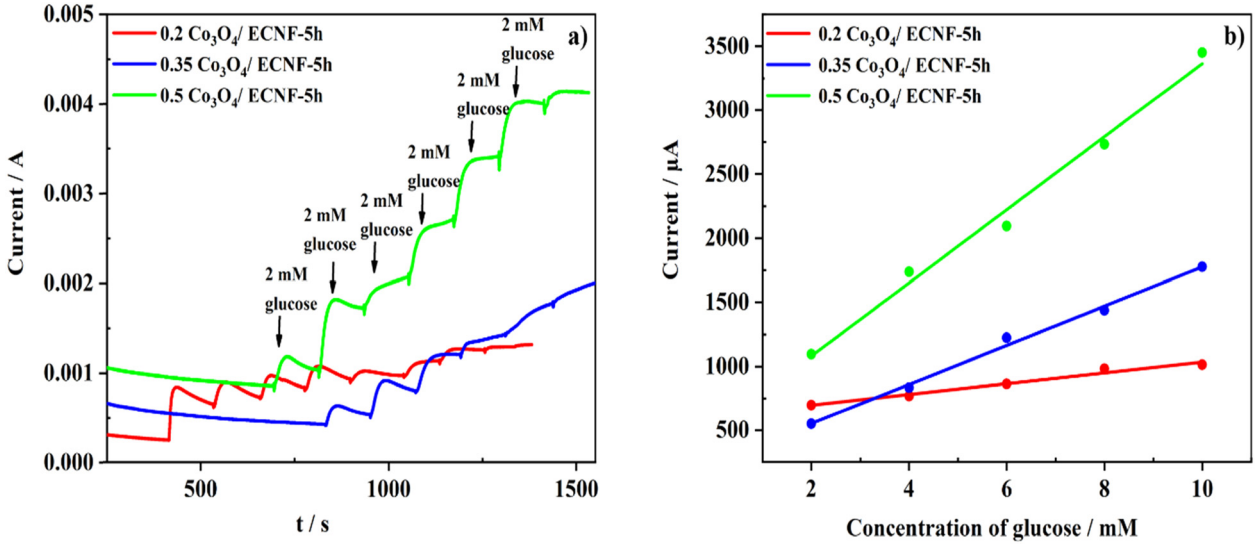

Figure 7: (a) CA plots of the Co_3O_4/ECNF electrodes with different concentrations of glucose in 0.1 M NaOH solution recorded at +0.55 V, and (b) calibration curves of the electrodes.

Table 2: Sensor parameters values of Co_3O_4/ECNF composite electrodes

Sample	Sensitivity ($\mu A \cdot mM^{-1} \cdot cm^{-2}$)	L.R. (mM)	LOD (mM)
0.2 Co_3O_4/CNF	70.46	2–10	0.93
0.35 Co_3O_4/CNF	254.85	2–10	0.61
0.5 Co_3O_4/CNF	475.72	2–10	0.82

Figure 7a depicts the CA plots of Co_3O_4/ECNF electrodes containing various amounts of metal salt precursor after sequential inclusion of glucose having a specified concentration of 2 mM at each time of addition. As it can be seen, an increment in the dose of CoAc resulted in the increase in the amperometric current response. In addition, based on the calibration plots of the samples presented in Figure 7b, with the increasing the amount of catalyst in the electrode, an increment took place in the slope of the calibration plot, resulting from the increased conductivity and also the surface area, which leads to the increase of the biosensor sensitivity respect to the glucose. Among the samples, 0.5 Co_3O_4/ECNF-5h electrode delivered the highest sensitivity (475.72 $\mu A \cdot mM^{-1} \cdot cm^{-2}$) (Table 2). Worth mentioning that in the range of 2–10 mM, all electrodes manifested a linear signal to the changes in the glucose concentration. Another merit of the electrodes is their LOD, which is less than 1.

Selectivity is considered a key parameter in the assessment of the free enzyme glucose biosensors' performance. For doing the selectivity test, ascorbic acid, uric acid, and dopamine were selected as interferences since they exist in the real sample of blood. Blood glucose levels in humans are approximately determined by 3–8 mM, whereas the concentration of the aforementioned interfering species is roughly 0.1 mM [51]. The CA analysis of the samples was carried out through the addition of glucose analyte and interfering agents successively into the 0.1 M NaOH electrolyte. According to Figure 8, 0.5 Co_3O_4/ECNF-5 h

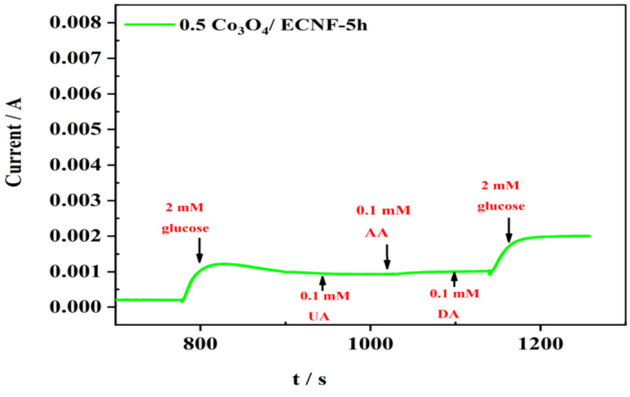

Figure 8: Amperometric response of Co_3O_4/ECNF composite electrode to the addition of 0.1 mM of different interferent's analytes in the presence of glucose analyte in 0.1 M NaOH solution.

Table 3: The comparison between our work and recent reported nonenzymatic glucose biosensors

Materials	Preparation method	Sensitivity ($\mu A \cdot mM^{-1} \cdot cm^{-2}$)	LR (mM)	LOD (mM)	Ref.
NiCFP	Electrospinning	420.4	0.002–2.5	1	[52]
Co_3O_4 nanofibers	Electrospinning	36.25	Up to 2.04	97×10^{-5}	[53]
Co_3O_4 UHMSA[a]	Hydrothermal	102.77	—	1.84×10^{-3}	[54]
Ni-CoO/CNF/GCE	Electrospinning	—	25×10^{-5} to 0.6	3×10^{-5}	[55]
Co_3O_4@PANINFs	Precipitation	14.25	0.1–8	0.06	[56]
Co_3O_4/SWCNTs/GCE	Hydrothermal	96.92	1–5	25×10^{-5}	[57]
Co_3O_4@Ag NWs-GR/NF[b]	Electrospinning	2.49	0.003–2	98×10^{-5}	[58]
0.5 Co_3O_4/CNF	Electrospinning	475.72	2–10	0.82	This work

[a] Urchin-like hollow microspheres self-supporting architecture.
[b] Graphene/Nickel foam.

composite electrode delivered no considerable current response toward the interfering agents, indicating that a superior selectivity toward the diagnosis of glucose is attained for the electrode in spite of the presence of interfering agents.

Moreover, our work has been compared to some recent glucose biosensors whose key parameters, including sensitivity, LOD, and LR are summarized in Table 3. Accordingly, the CO_3O_4/ECNF glucose biosensor possesses excellent electrochemical properties and can detect glucose analytes with superior sensitivity.

4 Conclusions

Co_3O_4/ECNF nanocomposite was synthesized through electrospinning the polymer and metal precursor, followed by the thermal treatment process for the reduction of metals and carbonization of PAN fibers. The carbonization process was performed at three different times including 1, 3, and 5 h, of which 5 h was selected as the optimum since, at this time, a superior dispersion of particles on the nanofibers was achieved. In addition, 5 g CoAc precursor was considered the optimal amount for the fabrication of Co_3O_4/ECNF electrode. CV measurements of the 0.5 Co_3O_4/ECNF-5 h electrode showed that by increasing the amount of glucose in the alkaline solution, the oxidation peak current increased, which is evidence of the good sensitivity of the electrode. Moreover, in accordance with the results obtained from the CV and EIS analyses, the redox reaction of glucose on the electrode is a diffusion-controlled process. Another merit making the 0.5 Co_3O_4/ECNF-5h composite electrode, an appropriate candidate to be used as an enzyme-free glucose biosensor is its excellent selectivity. This electrode delivered no considerable current response toward the interfering agents, implying that the electrode showed a superior selectivity to the diagnosis of the target analyte in the presence of interfering species.

Acknowledgments: This work was supported by the National Research Foundation of Korea (NRF) grant funded by the Korea government (MSIT) (No. 2022M3J7A1062940).

Funding information: The Authors state no funding involved.

Author contributions: Conceptualization, A. Mohammadpour-Haratbar; methodology, A. Mohammadpour-Haratbar; writing–original draft preparation, A. Mohammadpour-Haratbar., B. Mosallanejad; writing–review and editing, A. Mohammadpour-Haratbar., B. Mosallanejad; supervision, Y. Zare; project administration, Y. Zare.

Conflict of interest: The Authors state no conflict of interest.

References

[1] Azlan, A. Y. H. N., H. Katas, M. F. M. Busra, N. A. M. Salleh, and A. Smandri. Metal nanoparticles and biomaterials: The multipronged approach for potential diabetic wound therapy. *Nanotechnology Reviews*, Vol. 10, 2021, pp. 653–670.

[2] Wang, Q., S. Zheng, T. Li, and Z. Wang. Ni/NiO multivalent system encapsulated in nitrogen-doped graphene realizing efficient activation for non-enzymatic glucose sensing. *Ceramics International*, Vol. 47, 2021, pp. 22869–22880.

[3] Karimi-Maleh, H., K. Cellat, K. Arikan, A. Savk, F. Karimi, and F. Şen. Palladium–nickel nanoparticles decorated on functionalized-MWCNT for high precision non-enzymatic glucose sensing. *Materials Chemistry and Physics*, Vol. 250, 2020, id. 123042.

[4] Garg, V., T. Gupta, S. Rani, S. Bandyopadhyay-Ghosh, S. B. Ghosh, L. Qiao, et al. A hierarchically designed nanocomposite hydrogel with multisensory capabilities towards wearable devices for human-body motion and glucose concentration detection. *Composites Science and Technology*, Vol. 213, 2021, id. 108894.

[5] Alhazmi, H. A., W. Ahsan, B. Mangla, S. Javed, M. Z. Hassan, M. Asmari, et al. Graphene-based biosensors for disease theranostics: Development, applications, and recent advancements. *Nanotechnology Reviews*, Vol. 11, 2022, pp. 96–116.
[6] Saini, D. Synthesis and functionalization of graphene and application in electrochemical biosensing. *Nanotechnology Reviews*, Vol. 5, 2016, pp. 393–416.
[7] Hassan, M. H., C. Vyas, B. Grieve, and P. Bartolo. Recent advances in enzymatic and non-enzymatic electrochemical glucose sensing. *Sensors*, Vol. 21, 2021, id. 4672.
[8] Sagadevan, S., M. M. Shahid, Z. Yiqiang, W. C. Oh, T. Soga, J. A. Lett, et al. Functionalized graphene-based nanocomposites for smart optoelectronic applications. *Nanotechnology Reviews*, Vol. 10, 2021, pp. 605–635.
[9] Abd Elkodous, M., H. M. El-Husseiny, G. S. El-Sayyad, A. H. Hashem, A. S. Doghish, D. Elfadil, et al. Recent advances in waste-recycled nanomaterials for biomedical applications: waste-to-wealth. *Nanotechnology Reviews*, Vol. 10, 2021, pp. 1662–1739.
[10] Tee, S. Y., C. P. Teng, and E. Ye. Metal nanostructures for non-enzymatic glucose sensing. *Materials Science and Engineering: C*, Vol. 70, 2017, pp. 1018–1030.
[11] Lee, W. C., K. B. Kim, N. G. Gurudatt, K. K. Hussain, C. S. Choi, D. S. Park, et al. Comparison of enzymatic and non-enzymatic glucose sensors based on hierarchical Au-Ni alloy with conductive polymer. *Biosensors and Bioelectronics*, Vol. 130, 2019, pp. 48–54.
[12] Shakhih, M. F. M., A. S. Rosslan, A. M. Noor, S. Ramanathan, A. M. Lazim, and A. A. Wahab. Enzymatic and non-enzymatic electrochemical sensor for lactate detection in human biofluids. *Journal of The Electrochemical Society*, Vol. 168, 2021, id. 67502.
[13] Othmani, A., M. Derbali, R. Kalfat, F. Touati, and H. Dhaouadi. A novel 1D/2D Bi_2S_3/g-C_3N_4 core–shell nanocomposite as a highly performing H_2O_2 non-enzymatic electrochemical sensor. *Journal of Materials Research and Technology*, Vol. 15, 2021, pp. 5762–5775.
[14] Kour, R., S. Arya, S. J. Young, V. Gupta, P. Bandhoria, and A. Khosla. Recent advances in carbon nanomaterials as electrochemical biosensors. *Journal of The Electrochemical Society*, Vol. 167, 2020, id. 37555.
[15] Sanati, A., M. Jalali, K. Raeissi, F. Karimzadeh, M. Kharaziha, S. S. Mahshid, et al. A review on recent advancements in electrochemical biosensing using carbonaceous nanomaterials. *Microchimica Acta*, Vol. 186, 2019, pp. 1–22.
[16] Chanda, S. and D. S. Bajwa. A review of current physical techniques for dispersion of cellulose nanomaterials in polymer matrices. *Reviews on Advanced Materials Science*, Vol. 60, 2021, pp. 325–341.
[17] Martínez-Pérez, C. A. Electrospinning: A promising technique for drug delivery systems. *Reviews on Advanced Materials Science*, Vol. 59, 2020, pp. 441–454.
[18] Kośla, K., M. Olejnik, and K. Olszewska. Preparation and properties of composite materials containing graphene structures and their applicability in personal protective equipment: A review. *Reviews on Advanced Materials Science*, Vol. 59, 2020, pp. 215–242.
[19] Ji, W., G. Zhao, C. Guo, L. Fan, H. Deng, R. Du, et al. A novel method to fabricate two-dimensional nanomaterial based on electrospinning. *Composites Part A: Applied Science and Manufacturing*, Vol. 143, 2021, id. 106275.
[20] Yu, S., Y. Zou, Q. Wang, J. Xu, C. Xiang, F. Xu, et al. Self-supported Co–Mo sulfide in electrospun carbon nanofibers as electrocatalysts for hydrogen evolution reaction in alkaline medium. *Journal of Alloys and Compounds*, 2022, id. 165094.
[21] Shakil, U. A., S. B. A. Hassan, M. Y. Yahya, and M. R. M. Rejab. A focused review of short electrospun nanofiber preparation techniques for composite reinforcement. *Nanotechnology Reviews*, Vol. 11, 2022, pp. 1991–2014.
[22] Kai, G., H. Miaohong, P. Wenhao, and W. Jinguo. Molecular dynamics of C–S–H production in graphene oxide environment. *Reviews on Advanced Materials Science*, Vol. 61, 2022, pp. 90–101.
[23] Barot, T., D. Rawtani, and P. Kulkarni. Nanotechnology-based materials as emerging trends for dental applications. *Reviews on Advanced Materials Science*, Vol. 60, 2021, pp. 173–189.
[24] Ali, A. M., M. Z. Omar, H. Hashim, M. S. Salleh, and I. F. Mohamed. Recent development in graphene-reinforced aluminium matrix composite: A review. *Reviews on Advanced Materials Science*, Vol. 60, 2021, pp. 801–817.
[25] Du, M., H. Jing, Y. Gao, H. Su, and H. Fang. Carbon nanomaterials enhanced cement-based composites: advances and challenges. *Nanotechnology Reviews*, Vol. 9, 2020, pp. 115–135.
[26] Power, A. C., B. Gorey, S. Chandra, and J. Chapman. Carbon nanomaterials and their application to electrochemical sensors: A review. *Nanotechnology Reviews*, Vol. 7, 2018, pp. 19–41.
[27] Meng, Q., Y. Huang, J. Ye, G. Xia, G. Wang, L. Dong, et al. Electrospun carbon nanofibers with *in-situ* encapsulated Ni nanoparticles as catalyst for enhanced hydrogen storage of MgH_2. *Journal of Alloys and Compounds*, Vol. 851, 2021, id. 156874.
[28] Cui, K., Y. Song, Q. Guo, F. Xu, Y. Zhang, Y. Shi, et al. Architecture of electrospun carbon nanofibers–hydroxyapatite composite and its application act as a platform in biosensing. *Sensors and Actuators B: Chemical*, Vol. 160, 2011, pp. 435–440.
[29] Zhu, H., L. Li, W. Zhou, Z. Shao, and X. Chen. Advances in non-enzymatic glucose sensors based on metal oxides. *Journal of Materials Chemistry B*, Vol. 4, 2016, pp. 7333–7349.
[30] Zhang, X., L. Zhang, H. Liu, B. Cao, L. Liu, and W. Gong. Structure, morphology, size and application of iron phosphate. *Reviews on Advanced Materials Science*, Vol. 59, 2020, pp. 538–552.
[31] Zhang, H., G. Chen, B. Yu, and H. Cong. Emerging advanced nanomaterials for cancer photothermal therapy. *Reviews on Advanced Materials Science*, Vol. 53, 2018, pp. 131–146.
[32] Liu, S., Z. Wang, F. Wang, B. Yu, and T. Zhang. High surface area mesoporous CuO: A high-performance electrocatalyst for non-enzymatic glucose biosensing. *RSC Advances*, Vol. 4, 2014, pp. 33327–33331.
[33] Li, Y., Y. Y. Song, C. Yang, and X. H. Xia. Hydrogen bubble dynamic template synthesis of porous gold for nonenzymatic electrochemical detection of glucose. *Electrochemistry Communications*, Vol. 9, 2007, pp. 981–988.
[34] Rick, J., M. C. Tsai, and B. J. Hwang. Biosensors incorporating bimetallic nanoparticles. *Nanomaterials*, Vol. 6, 2015, id. 5.
[35] Naresh, V. and N. Lee. A review on biosensors and recent development of nanostructured materials-enabled biosensors. *Sensors*, Vol. 21, 2021, id. 1109.

[36] Mohammadpour-Haratbar, A., S. Mazinani, F. Sharif, and A. M. Bazargan. Improving Nonenzymatic Biosensing Performance of Electrospun Carbon Nanofibers decorated with Ni/Co Particles via Oxidation. *Applied Biochemistry and Biotechnology*, Vol. 194, 2022, pp. 1–23.

[37] Sharma, A., S. Arya, D. Chauhan, P. R. Solanki, S. Khajuria, and A. Khosla. Synthesis of Au–SnO_2 nanoparticles for electrochemical determination of vitamin B12. *Journal of Materials Research and Technology*, Vol. 9, 2020, pp. 14321–14337.

[38] Mohammadi, M. A., F. A. Tabar, A. Mohammadpour-Haratbar, A. M. Bazargan, S. Mazinani, A. H. Keihan, et al. Preparation and evaluation of electrospun carbon nanofibers infused by metal nanoparticles for supercapacitor electrodes application. *Synthetic Metals*, Vol. 274, 2021, id. 116706.

[39] Bazargan, A. M., M. Esmaeilpour, and M. Keyanpour-rad. Catalytically Graphitized Electrospun Carbon Nanofibers Adorned with Nickel Nanoparticles for Catalysis Applications. *Journal of Nanostructures*, Vol. 6, 2016, pp. 52–57. doi: 10.7508/JNS.2016.01.008

[40] Abouali, S., M. Akbari Garakani, B. Zhang, Z. L. Xu, E. Kamali Heidari, J. Huang, et al. Electrospun carbon nanofibers with *in situ* encapsulated Co_3O_4 nanoparticles as electrodes for high-performance supercapacitors. *ACS Applied Materials and Interfaces*, Vol. 7, 2015, pp. 13503–13511.

[41] Chen, S., S. Fu, D. Liang, X. Chen, X. Mi, P. Liu, et al. Preparation and properties of 3D interconnected CNTs/Cu composites. *Nanotechnology Reviews*, Vol. 9, 2020, pp. 146–154.

[42] Mohammadpour-Haratbar, A., P. Kiaeerad, S. Mazinani, A. M. Bazargan, and F. Sharif. Bimetallic nickel–cobalt oxide nanoparticle/electrospun carbon nanofiber composites: Preparation and application for supercapacitor electrode. *Ceramics International*, Vol. 48, No. 7, 2022, pp. 10015–10023.

[43] Li, L., M. Liu, S. He, and W. Chen. Freestanding 3D mesoporous Co_3O_4@ carbon foam nanostructures for ethanol gas sensing. *Analytical Chemistry*, Vol. 86, 2014, pp. 7996–8002.

[44] Liu, F., P. Wang, Q. Zhang, Z. Wang, Y. Liu, Z. Zheng, et al. Porous Co_3O_4 nanosheets as a high-performance non-enzymatic sensor for glucose detection. *Analytical and Bioanalytical Chemistry*, Vol. 410, 2018, pp. 7663–7670.

[45] Xu, H., C. Xia, S. Wang, F. Han, M. K. Akbari, Z. Hai, et al. Electrochemical non-enzymatic glucose sensor based on hierarchical 3D Co_3O_4/Ni heterostructure electrode for pushing sensitivity boundary to a new limit. *Sensors and Actuators B: Chemical*, Vol. 267, 2018, pp. 93–103.

[46] Cheng, S., S. DelaCruz, C. Chen, Z. Tang, T. Shi, C. Carraro, et al. Hierarchical Co_3O_4/CuO nanorod array supported on carbon cloth for highly sensitive non-enzymatic glucose biosensing. *Sensors and Actuators B: Chemical*, Vol. 298, 2019, p. 126860.

[47] Chang, A. S., N. N. Memon, S. Amin, F. Chang, U. Aftab, M. I. Abro, et al. Facile Non-enzymatic Lactic Acid Sensor Based on Cobalt Oxide Nanostructures. *Electroanalysis*, Vol. 31, 2019, pp. 1296–1303.

[48] Hasanzadeh, M., G. Karim-Nezhad, N. Shadjou, M. Hajjizadeh, B. Khalilzadeh, L. Saghatforoush, et al. Cobalt hydroxide nanoparticles modified glassy carbon electrode as a biosensor for electrooxidation and determination of some amino acids. *Analytical Biochemistry*, Vol. 389, 2009, pp. 130–137.

[49] Kaçar, C., B. Dalkiran, P. E. Erden, and E. Kiliç. An amperometric hydrogen peroxide biosensor based on Co_3O_4 nanoparticles and multiwalled carbon nanotube modified glassy carbon electrode. *Applied Surface Science*, Vol. 311, 2014, pp. 139–146.

[50] Dalkiran, B., C. Kacar, P. E. Erden, and E. Kilic. Amperometric xanthine biosensors based on chitosan-Co_3O_4-multiwall carbon nanotube modified glassy carbon electrode. *Sensors and Actuators B: Chemical*, Vol. 200, 2014, pp. 83–91.

[51] Park, S., H. Boo, and T. D. Chung. Electrochemical non-enzymatic glucose sensors. *Analytica Chimica Acta*, Vol. 556, 2006, pp. 46–57.

[52] Liu, Y., H. Teng, H. Hou, and T. You. Nonenzymatic glucose sensor based on renewable electrospun Ni nanoparticle-loaded carbon nanofiber paste electrode. *Biosensors and Bioelectronics*, Vol. 24, 2009, pp. 3329–3334. doi: 10.1016/j.bios.2009.04.032

[53] Ding, Y., Y. Wang, L. Su, M. Bellagamba, H. Zhang, and Y. Lei. Electrospun Co_3O_4 nanofibers for sensitive and selective glucose detection. *Biosensors and Bioelectronics*, Vol. 26, 2010, pp. 542–548.

[54] Ding, L., M. Zhao, S. Fan, Y. Ma, J. Liang, X. Wang, et al. Preparing Co_3O_4 urchin-like hollow microspheres self-supporting architecture for improved glucose biosensing performance. *Sensors and Actuators B: Chemical*, Vol. 235, 2016, pp. 162–169.

[55] Mei, Q., R. Fu, Y. Ding, A. Wang, D. Duan, D. Ye, et al. Electrospinning of highly dispersed Ni/CoO carbon nanofiber and its application in glucose electrochemical sensor. *Journal of Electroanalytical Chemistry*, Vol. 847, 2019, id. 113075.

[56] Yassin, M. A., B. K. Shrestha, R. Ahmad, S. Shrestha, C. H. Park, and C. S. Kim. Exfoliated nanosheets of Co_3O_4 webbed with polyaniline nanofibers: A novel composite electrode material for enzymeless glucose sensing application. *Journal of Industrial and Engineering Chemistry*, Vol. 73, 2019, pp. 106–117.

[57] Liaqat, I., N. Iqbal, M. Aslam, M. Nasir, A. Hayat, D. X. Han, et al. Co_3O_4 nanocubes decorated single-walled carbon nanotubes for efficient electrochemical non-enzymatic glucose sensing. *SN Applied Sciences*, Vol. 2, 2020, pp. 1–12.

[58] Zhao, Z., Y. Huang, Q. Li, H. Mei, F. Zhu, and W. Gong. Electrochemical glucose sensitive device based on graphene supported Co_3O_4@ Ag NWs core-shell nanostructures. *Applied Surface Science*, Vol. 565, 2021, id. 150553.